ISSN 0915-633X

NATIONAL INSTITUTE FOR FUSION SCIENCE

LHD Helical Divertor

N. Ohyabu, T. Watanabe, Hantao Ji, H. Akao, T. Ono,
T. Kawamura, K. Yamazaki, K. Akaishi, N. Inoue, A. Komori,
Y. Kubota, N. Noda, A. Sagara, H. Suzuki, O. Motojima,
M. Fujiwara, A. Iiyoshi

(Received – July 8, 1993)

NIFS-239 July 1993

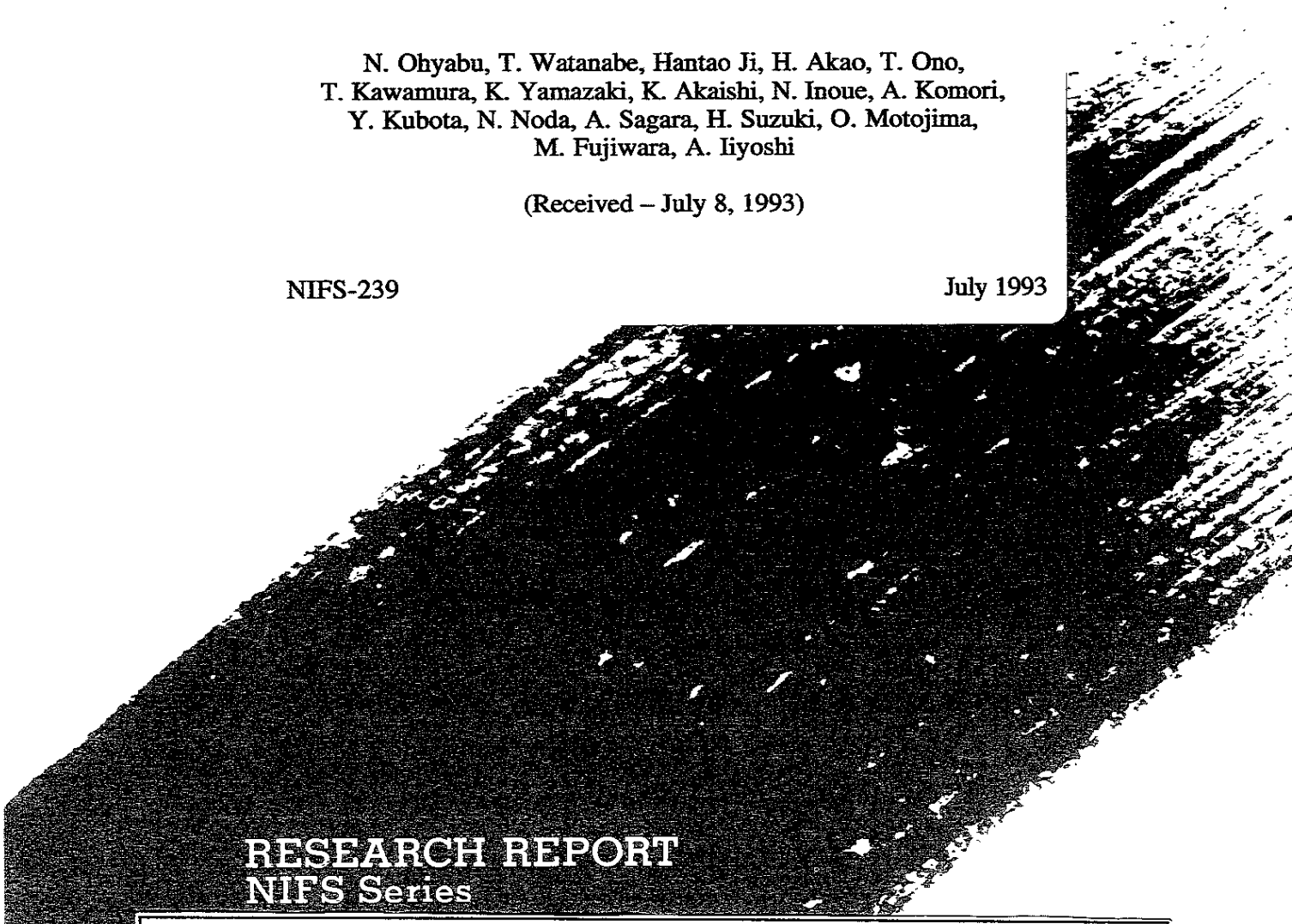

RESEARCH REPORT
NIFS Series

NAGOYA, JAPAN

LHD HELICAL DIVERTOR

N.OHYABU, T.WATANABE, HANTAO JI, H.AKAO[1)], T.ONO[2)], T.KAWAMURA, K.YAMAZAKI, K.AKAISHI, N.INOUE, A.KOMORI, Y.KUBOTA, N.NODA, A.SAGARA, H.SUZUKI, O.MOTOJIMA, M.FUJIWARA, A.IIYOSHI.

National Institute for Fusion Science, Nagoya, 464-01, Japan

1) NEC Inc. 2) Nagoya University

ABSTRACT. The Large Helical Device (LHD) now under construction is a heliotron/torsatron device with a closed divertor system. The edge LHD magnetic structure has been studied in detail. A peculiar feature of the configuration is existence of edge surface layers, a complicated three dimensional magnetic structure which does not, however, seem to hamper the expected divertor functions. Two divertor operational modes are being considered for the LHD experiment, high density, cold radiative divertor operation as a safe heat removal scheme and high temperature divertor plasma operation. In the latter operation, a divertor plasma with temperature of a few kev, generated by efficient pumping, expects to lead to significant improvement in core plasma confinement. Conceptual designs of the LHD divertor components are under way.

Keywords:

Large Helical Device, LHD, heliotron/torsatron, divertor, high temperature divertor opeartion, confinement enhancement, radiative heat removal,

1. INTRODUCTION

Recently significant progress has been made in the stellarator or helical system research. With the inherent advantage of stellarator as an attractive steady state reactor, there has been growing interest in stellarator in the fusion community. The National Institute for Fusion Science (NIFS) has decided to build a large, l=2 heliotron/torsatron type device, called the Large Helical Device (LHD), aimed at demonstrating the attractiveness of the helical device at more reactor relevant plasma parameters [1,2]. The LHD device parameters are : R (the major radius) = 3.9 m, a (the minor radius) = 0.6 m, m (the toroidal mode number of the helical coil) = 10, γ_c (the pitch of the helical coils) = 1.25 , α_c (the pitch modulation of the helical coils) = 0.1 . It is a superconducting coil device and thus steady state plasma operations will be demonstrated provided that the impurity contamination is kept low. For this purpose, a kind of divertor is believed to be required for the impurity control. The divertor is, also critically important in enhancing the core energy confinement. The LHD τ_E scaling (the most widely accepted empirical energy confinement scaling for stellarators) [3] predicts that a factor of 2-3 improvement is needed to have ignition in helical devices with reasonable size (R ~ 20 m). Thus enhancement of the energy confinement by the divertor is one of the major experimental subjects in the LHD program.

A build-in divertor configuration exists for heliotron/torsatron type devices. This advantage has not been explored in any existing devices partly because a full divertor configuration makes the device larger and hence more costly. The divertor configuration requires 1) a clearance between the first wall and the plasma. 2) a large vacuum vessel needed to accommodate the divertor chamber. We are designing a helical divertor which satisfies these requirements and it will be the first helical divertor experiment which will

demonstrate various divertor functions which enhance the plasma quality, as observed in the tokamak divertor experiments.

During the last decade, the tokamak divertor experimental studies have demonstrated a few important functions in addition to the impurity control or shielding, which has been once considered as the major divertor function. The Doublet III group proposed " expanded boundary" divertor configuration in which the divertor channel are expanded magnetically by an elaborated poloidal coil system [4]. The large expanded volume in turn provides a cold, radiative plasma boundary region where most of the heat flow from the core is converted into the impurity radiation power before reaching the divertor plate. Subsequently the Doublet III experiment showed that a very high density plasma with even higher than the central core density exists stably near the divertor plate [5] and also demonstrated that under certain conditions for the Ohmically heated discharges, the majority of Argon impurities, injected externally accumulates in the divertor channel [6].

High power heating experiments in tokamaks and helical devices have shown that the energy confinement deteriorates with increasing heating power, the major physics concern in the present experimental research. With divertor function on, the energy confinement in tokamaks improves by a factor of ~ 2 (so called H-mode) [7] and thus the divertor becomes an essential component for successful tokamak operations. Edge recycling control by the divertor appears to be the key to trigger and maintain the H-mode phase.

One of the goals of the LHD divertor experiments is to demonstrate the divertor functions, achieved in the tokamak experiments. In designing the LHD divertor, special cares have been taken for this purpose. In addition to those functions, we plan to explore more advanced divertor concept (high temperature divertor operation). In this operation, high temperature divertor plasma is maintained by avoiding particle recycling as much as possible. This is accomplished by efficient pumping in the divertor. When the edge

temperature exceeds a value of the temperature seen at the H-mode pedestal (a few cm inside the separatrix) i.e., 300 -1000 eV, we expect that core confinement improves similarly as formation of the high temperature pedestal leads to the core confinement enhancement in tokamak H-mode discharges.

Divertor geometry in the LHD is discussed in Section II and conceptional designs for the divertor chamber geometry and divertor components are depicted in Section III. Section IV deals with two important operational modes, cold radiative operational mode and high temperature operational mode.

II. MAGNETIC CONFIGURATION OF THE LHD DIVERTOR

Divertor magnetic configurations in heliotron/torsatron type helical devices such as LHD are basically the same as those in tokamaks in a sense that the particle and heat flux diffusing out from the core plasma region are magnetically guided to the divertor chamber. Divertor function requires magnetic separation of closed and open surface regions, which in turn requires a kind of "X-point". In tokamak poloidal divertor configurations, there exists a clear separatrix (a flux surface with X-point) which sharply separates a closed surface region in which plasma is confined and a open region which is connected to the divertor plates through the field lines. In toroidal heliotron/torsatron configurations, toroidal effects make the separatrix surface fairly vague. For the LHD configuration, there exist three distinctly different edge regions as is shown in Fig. 1(a) : (1) the region of the magnetic island layers and stochastic structure, which surrounds the closed surface region, (2) the region with thin curved plasma layers, a characteristic of the divertor configuration of heliotron/torsatron type and (3) the divertor channel beyond the X-point.

X-point Region

The LHD divertor geometry at the poloidal plane (i.e.,constant ϕ plane) is shown in Fig.1(a) ,but is not easy to understand it since the divertor regions are helically twisted as the helical coils. When one see the divertor structure along the helical direction as in Fig. 1(b), its structure looks like that of the tokamak, a more familiar configuration and becomes easier to understand it. But the divertor geometry exhibits a strong poloidal variation, e.g. the width of the divertor chamber varys from 1200 mm at $\theta = 0^{\circ}$ to 400 mm at $\theta = 180^{\circ}$.

In Fig. 1(c), the direction of the field line on the plane perpendicular to the helical direction is also shown by arrows. The length of the arrow is proportional to strength of the magnetic field on the plane normalized by that of the magnetic field along the helical direction. The X-point rotates with nearly the same pitch as the helical coils and the normalized field is zero at the X-point. The normalized field is of the order of unity in the divertor channel beyond the X-point and hence the distance between the X-point and divertor plate is very short, of the order of the plasma minor radius.

In a straight heliotron/torsatron configuration, the X-point is clearly defined and its radial position does not varies as it rotates helically. This is no longer true for toroidal heliotron/torsatron configurations. Referring Fig. 1(a), a local rotational transform (defined by (B_θ / B_ϕ) (R/r)) on the horizontal axis is much higher than the rotational transform (the flux surface average transform) and increases with radius (r) and becomes equal to that of the helical coil at the X-point. Near the X-point, increase of the local rotational transform is due to decrease of B_ϕ with increasing r. It is quite contrary to the conventional stellarator configurations where it is due to increase of B_θ. Radial position of the X-point varies substantially with poloidal or toroidal angle, as shown in Fig.2. This radial motion of the X-point is a key in generating structure of edge surface layers, as described later.

Magnetic Island and Stochastic Structure

In the region (1), several island layers with toroidal mode number of 10 are imbedded and with increasing radius, poloidal mode number of the island layers decreases and size of the island increases. Eventually the layers overlap, resulting in a stochastic field structure. Thus definition of the outermost flux surface is vague. These islands are not generated by the error fields due to inaccuracy in coil manufacturing or installation and thus are called "natural" islands. Generally the width of the stochastic region is sensitive to the position of the plasma axis and the shape of the plasma.

Edge Surface Layer Region

Beyond the stochastic region , there exists an region with multiple thin curved layers (edge surface layer region). Fig.1(a) shows a puncture plot of the field line tracing with starting points just within the stochastic region. The basic structure of the puncture plots is independent of the initial starting points as long as they are within the stochastic region or on the edge surface layers close to the stochastic region. Field lines in the stochastic region enter these surface layers and after many toroidal circulations, they reach the X-point and then hit the divertor plate. The existence of such edge layers is a peculiar feature of heliotron/torsatron divertor configurations. This structure is created by radial movement of the X-point (Fig.2) and high local rotational transform and high local shear at the edge of the large major radius side of the torus ($\pi/2 > \theta > -\pi/2$).

The field line movement is illustrated in Fig. 3. Consider field lines starting from the outer most thin curved layer labeled "1" in Fig.3(b). As they travel in the parallel direction by one toroidal pitch (36 ° toroidally), they rotate poloidally just as those inside the closed surface region do, moving on to the adjacent thin curved layer labeled "2". However, ones near the wall reach the wall. When the field line in the layers move into the region with $3\pi/2 < \theta < 2\pi$, the X-point moves towards the layers and the field lines are pulled towards the X-point, bending the surface layers (labeled "3") . Field

lines near the tip of the bent layer (e.g. field line C) are pulled to the wall. The rest of field lines on the layer do not escape to the wall. The field line B and D rotate poloidally faster than field line A and E because of their larger radii and hence higher local rotational transform. In this process, a sort of mixing takes place. Before mixing, Field line A is located at the largest radius and the largest poloidal angle θ among the five field lines. After this process, it locates at smaller radius and smaller poloidal angle than field line D, which locates at smaller radius before the mixing. Such folded layers are stretched into a very thin layer because of very high local rotational transform and high local shear on the larger major radius side of the torus. For the standard configuration, the plasma is shifted outward to improve the MHD stability, as shown in Fig.3(a) and thus the distance between the last closed surface and the X-point is shorter on the larger major radius side and hence the local rotational transform and shear are higher. Finally it becomes a "starting" layer, labeled "1" at the poloidal plane different from one with the real starting layer. In Fig. 3, field lines are traced forwards. If they are traced backwards, the pictures of Fig. 3 becomes up side down with respect to the midplane. With such a generation mechanism of the layer, any edge surface layer consists of multiple, extremely stretched layers, which themselves are a group of multiple layers, i.e., the layer has a structure similar to one, shown in the rectangle box on Fig.3(a) if the layer is expanded perpendicularly.

Field lines in these layers do not escape to the wall in a short distance. This is shown in Fig.4 which plots the connection length as a function of the starting position of the field line tracing. The connection length is the distance between the starting point and the divertor plate or wall and the starting points are located on the outer midplane ($Z = 0$, $3.35\ m < R < 3.47\ m$). We found that the positions at which the connection length is long correspond to the layers. Referring to Fig.1(a), there exists regions without puncture points between the layers, meaning that the field lines in these regions are not

connected to the stochastic region. Instead they are connected to the divertor plates when they are traced forwards and backwards. A group of the field lines in region 0 moves into region 1 after one toroidal pitch (36 ° toroidal rotation) and move into region 2 and so on, finally reaching the divertor plate. If field line is followed backwards, those in region 0 move back into region -1 after 36° backward toroidal rotation and move into region -2 and so on, reaching the divertor plate.

When plasma particles and heat flow along the field line, they also cross the field line. To study the effect of the plasma cross field transport in such a complicated three dimensional divertor magnetic structure, the field lines are traced with a random walk process (at every 0.2 m step, positions of the field lines deviate by δ in the plane perpendicular to the field lines with random azimuthal directions from the stochastic region until reaching a helical surface , defined by $\theta = -[5\phi + \theta_0 + 0.1 \sin(5\phi+\theta_0)]$. Here θ_0 is a constant, chosen to make the poloidal angle difference between the surface and the helical coil center surface 57° (see Fig.6(b)). The positions of the field line puncture point on this surface is close to the divertor plates which will be located at r~1.55 m. Thus puncture plots of the field lines on this helical surface are useful in estimating the spatial distributions of the particle and heat flows on the divertor plate and are shown in Fig. 5. A strong poloidal asymmetry is seen in the plots. The fine structure of the edge surface layer is clearly seen when it is traced exactly, i.e. $\delta = 0$. For a random walk process with $\delta = 1.2$ mm corresponding to a perpendicular diffusion coefficient of 0.5 m^2/s for a plasma with a temperature of 100 eV, i.e. a value that is slightly smaller than a typically observed edge value, the fine structure is smoothed out completely. We expect that the distributions of the heat and particle fluxes for the LHD experiments are close to those with $\delta = 1.2$ mm. If so, the maximum heat flux on the divertor plate with a field line incident angle of 65° is expected to be ~ 5 MWm^{-2} for a standard 20 MW LHD discharge.

In a heliotron/torsatron configuration, there exists a nearly elliptical

shaped boundary (here we call it "separatrix boundary")[8], beyond which the field lines are connected to the divertor plate within one or two toroidal pitches. Beyond the separatrix boundary, the close surface region cannot exist. When we moves the plasma outward from the standard case (Δ =-0.15 m) by 0.15 m, the closed surface region is scraped by the separatrix boundary and the plasma area becomes smaller, as shown in Fig.6(c). The separatrix boundary, on the other hand does not change much (only a few cm) because required change of the vertical field strength is only a few percent of the total field when the plasma axis (Δ) is changed from Δ = 0 m to Δ = -0.2 m. The above mentioned edge surface layers exists between the stochastic region surrounding the closed region and the separatrix boundary. The size of this layer region varies when the plasma position is changed. When the position of the axis is 0.2 m, the volume of the closed surface region becomes maximum and the layer region becomes narrow. Such a configuration with maximum plasma volume is not as good as the standard one in terms of others properties such as the MHD stability. When $\Delta \sim 0$, the plasma boundary is more vague and the width of the edge surface layer region is wider as seen in Fig.1(a),6(c).

III Conceptual Design of the LHD Helical Divertor

One of the necessary conditions for divertor to function is that the edge plasma does not touch the first wall surrounding the main plasma. In the LHD configuration, the plasma is shifted inwards by ~ 0.2 m relative to the center of the two helical coils due to the toroidal effect and thus the distance between the coil center and the plasma edge on the small major radius side of the torus is fairly small. For the LHD design, it is 315 mm and the space allocation between the coil and the edge of the plasma are shown in Fig.7. In order to increase the gap between them, we have chosen helical coils with a high

current density of 53 A/mm^2 so that the width of the coil is reduced. Because of the superconducting coil system, a space for the thermal insulation gap and the thermal displacement of the components needs to be greater than 50 mm, making the space even tighter.

As discussed above, the position of the edge plasma (the outermost edge surface layer) does not move much even if the plasma axis is changed. To increase the gap distance, the geometry of the helical coil need to be changed. One way to do so is to add a modulation(α_c) of the helical coil winding ($\theta = 5\phi + \alpha_c \sin 5\phi$). For configurations similar to LHD, adding positive α_c by 0.1 gives an extra gap of 20 mm. For this reason, we have decided to add a small pitch modulation of $\alpha_c = 0.1$. For higher α_c, the gap increases further, but other properties start to deteriorate. After optimization of the system, the gap between the first wall and the plasma (the outermost edge surface layer) becomes 15 mm, a gap wide enough for the divertor to function well. The gap also depend on the coil pitch (γ_c). The standard γ_c was selected to be 1.25 for the LHD configuration judging from various physics considerations including the gap requirement. But it may be required to change the gap for the experimental study. The value of γ_c can be varied in the LHD since the helical coils have three layers, in which currents can be controlled independently. The standard case ($\gamma_c = 1.25$) corresponds to full current in the each layer and hence the maximum field (4T). By driving less current in the outermost layer, γ_c can be reduced, correspondingly lower maximum field. For example, when the γ_c is reduced from 1.25 to 1.23, the gap increases from 15 mm to 35 mm and correspondingly the maximum axis field decreases from 4T to 3.5T. As γ_c increases, the outer most thin layer starts to touch the first wall and the plasma heat and particle hit the first wall. In order to find how deeply the first wall must be inserted before all the field lines, starting from the stochastic region are intercepted by the first wall, we change the first wall position on the inner midplane, as shown in Fig.4. When the first wall is located at R = 3.385 m, scraping the outermost edge surface layer, less than

10% of the hitting spots of the field lines are on the first wall and the remaining field lines reach the divertor plate. When the wall is located at R = 3.41 m and hence scrapes the two outer most edge surface layers, then more than 90 % of the field lines hit the first wall, becoming almost a full limiter configuration.

The connection length beyond the outermost surface layer is very short, a few m and thus perpendicular spreading of plasma beyond the layer should be much narrower than the thickness of the scrape-off layer in comparable sized tokamak divertor configurations, typically ~ 10 mm. Accordingly, with the gap between the first wall and the outermost edge surface layer of ~ 15 mm, the majority of the heat and particle fluxes from the core are guided to the divertor plates installed in the divertor chamber as illustrated in Fig.1(a).

Divertor performance depends on how well the neutrals recycled at the divertor plates are controlled. For high temperature divertor operation discussed in Section IV, pumping efficiency in the divertor chamber is the key for the operation. The width of the entrance to the divertor chamber needs to be as small as possible for high pumping efficiency. In fact, pumping efficiency is the ratio of the entrance area to the "equivalent" pump surface area. We are considering a cryopump system with overall pumping efficiency of ~ 20 % for this purpose. We are also developing other pumping schemes with even higher efficiency, which will be reported elsewhere.

For high recycling operation, plasma plugging plays a crucial role. The plugging efficiency (η) is defined as a fraction of the neutral particle flux from the divertor plate being ionized by the plasma in the divertor channel. To estimate the plugging efficiency in the LHD divertor configuration, we use a neutral particle code (DEGAS [9]). A simple divertor model geometry shown in Fig.8(a) is used in the numerical estimation. In this model, the plasma particles with a density of n_{div} flows through the divertor channel with a width of Δ_p and recycle at the divertor plate. We assume that all the

particles be neutralized there and return as neutral particles. A fraction (η) of the neutral particles are ionized in the divertor channel within the divertor chamber. The rest of the particles escape the divertor chamber through the divertor slit (entrance). The plugging efficiency is found to be a function of $n_{div}\Delta_p$ and Δ_{slit} / d, being insensitive to the detailed divertor structure. Here Δ_{slit} and d are the width of the divertor slit and the depth of the divertor chamber, respectively. It increases with increasing $n_{div}\Delta_p$ and with decreasing Δ_{slit} / d. Fig.8(b) shows that plugging efficiency increases with density and the required divertor density for more than 70% plugging efficiency is around 1×10^{13} cm^{-3} for the LHD parameter conditions. Fig.8(c) shows that it decreases with increasing Δ_{slit} and the required Δ_{slit} for 70 % plugging efficiency is about 6 cm for the case (d = 15 cm, $n_{div}\Delta_p = 2.5\times10^{13}$ cm^{-2}). It is rather low compared with those in existing tokamak divertors in which poloidal expansion of the divertor channel helps to enhance the plasma plugging [10]. As discussed in the next section, ionization in the edge surface layers which surrounds the main plasma is expected to enhance the overall plugging efficiency up to 90 %. These calculations using a simplified divertor geometry provides a crude estimate of the plugging efficiency and more detailed calculations in a geometry, close to the real one are planned.

As discussed, the divertor performances are sensitive to Δ_{slit} / d. The width of the entrance is determined by the thickness of the divertor channel and movement of the divertor channel with Δ. The position change associated with change of the plasma axis from Δ = 0.0 to Δ = -0.20 m is minimal, less than 20 mm. On the large major radius side of the torus, a large space is available for the divertor chamber (d = 400 mm) and Δ_{slit} needs to be as large as 140 mm because of thicker edge surface layers, as clearly seen in Fig. 1(a). On the small major radius side, the space for the divertor chamber is very tight (d = 200 mm), but fortunately the width of the divertor channel is narrow and Δ_{slit} of 50 mm is acceptable. In any case, Δ_{slit} / d can be designed to be ~ 1/3, which is used as a model case in estimating the plugging efficiency

in Fig.8.

The divertor plates are the major divertor components which handle the heat flux from the core plasma. Its conceptual design has been completed. In the LHD divertor configuration, the direction of the magnetic field is nearly poloidal. All of four divertor legs have a three dimensional helical structure. From these facts, each divertor plate is designed as a helically running discrete-bar array. The angles between the field lines and the surfaces are designed to be around 25 degree at the striking points. Each bar is made of copper cooling channel, on which several pieces of graphite or C-C composite armor are directly brazed. The cylindrical bar is 34~40 mm in diameter, 300~400 mm in length and a total of 2040 bars is necessary for covering all the striking points of the four divertor legs. Pressurized water cooling will be used to keep the surface temperature of the armor below 1200 C^{o} under the maximum heat flux of 10 MW/m^2.

IV Divertor Operational Modes

We are considering two physics operational modes, low temperature, radiative plasma operation and high temperature divertor plasma operation modes.

Low Temperature Radiative Divertor Plasma Operation

Low temperature radiative divertor plasma operation create a cold, radiative plasma with high density in the divertor channel, which converts the power flux from the core region into the impurity radiative power, the most benign form of the heat removal. The condition for high density divertor plasma is described by

$$\lambda_e / L \quad < \quad 0.8\ (m/M)^{1/2}\ \gamma \qquad (1)$$

where m and M are electron and ion mass respectively and γ is the heat

transmission coefficient at the sheath. Here λ_e and L are electron mean free path and the field line length between the open surface region just outside the main plasma and the divertor plate respectively. This condition means that the electron parallel thermal diffusivity ($\chi_e = 3.16\lambda_e(kT/m)^{1/2}$) is not large enough to maintain $\nabla_{||}T = 0$ along the field line. Once the temperature drops nears the divertor plate, the density there increases because of constant pressure along the field line. The key divertor condition for the low temperature operation is high plasma plugging efficiency. In order to satisfy the condition (1), the recycling at the divertor plate must be enhanced to lower the temperature and hence λ_e. This can always be accomplished by increasing the particle flux from the core (Γ°) through the gas puffing, even though it is accompanied by increase in the average plasma density. But for most of the discharges, the average density is set by other considerations and thus control of leakage of the neutral particle flux from the divertor chamber into the main plasma region, is necessary to operate the high recycling divertor operation at the desired average density. With a given average density, Γ° depends on the particle transport coefficient and the particle deposition profile. Shallow particle fuelling such as gas puffing or natural recycling increase Γ° and hence is desirable for this operation. Furthermore with ionization of the recycled neutrals in the open region, the particle flux to the divertor plate is amplified by $\alpha = 1/(1-\eta)$. Here η is the plasma plugging efficiency which is defined as a fraction of neutral flux recycled from the plate being ionized in the open plasma region. With amplification α, the divertor temperature (T_{div}) scales as $Q_{div} / (\alpha\Gamma^\circ)$ and the divertor density (n_{div}) scales as $(\alpha\Gamma^\circ)^{3/2} / Q_{div}^{1/2}$ where Q_{div} is the heat flux to the divertor plate. Here we assume that $\Gamma_{div} \sim n_{div}T_{div}^{1/2}$ and $Q_{div} \sim \Gamma_{div}T_{div}$. The electron mean free path (λ_e) is decreases rapidly with α, $\lambda_e \sim Q_{div}^{5/2} / (\alpha\Gamma^\circ)^{7/2}$. Condition (1) becomes $\alpha\Gamma^\circ > C\, Q_{div}^{5/7} / L^{2/7}$ where C is a constant. From this Inequality, higher α is necessary to satisfy the high density divertor plasma condition. This seems to suggest that L appears not to

be a sensitive parameter for this condition because of its weak power dependence. But it is not the case because α is very sensitive to L. Large L and hence large divertor plasma volume generally provides high plugging efficiency and hence high α. This generally makes it difficult to achieve this type of operation in small devices.

Next we estimate the edge parameters for an LHD high recycling operation. The total power flux to the divertor plate is given as $Q_{div} = \gamma T_{div} n_{div} C_s S$ where S is the effective heat load surface area perpendicular to the field line. For the LHD divertor configuration, the thickness of the divertor channel layer (Δ_p) at the divertor region is ~20 mm. Assuming that heat and particle fluxes are localized in a 1/3 of the divertor area as seen in Fig.5, the total area (S) becomes ~ 1 m^2. When the divertor temperature and density are 40 ev and 1×10^{13} cm^{-3} respectively, the total heat and particle fluxes are 20 MW and 4×10^{23} / sec respectively. The electron mean free path is 2 m and the total field line length length must be above 20 m to satisfy the high recycling condition (1). Then an important question is raised what is the connection length for the LHD configuration. The field line length between the X-point and the divertor plate is very short (~1m), but it is not a relevant length. If one consider derivation of condition (1), the major assumptions are the constant pressure and dominance of the electron thermal conduction along the field line. These assumptions are expected to be satisfied even in the edge surface layers and thus the effective connection length can be several toroidal circulations (much greater than 20 m). Thus the high recycling condition will be satisfied when the divertor density is 1×10^{13} cm^{-3}. The choice of the divertor temperature and density also depends on the particle flux from the core and the plugging efficiency of the divertor. The above choice corresponds to the LHD plasma conditions, i.e., Q_{div} = 20 MW and $\Gamma_{div} = 4 \times 10^{23}$ / sec (the particle confinement time ~10 msec , the average core density ~ 5×10^{13} cm^{-3}, the plugging efficiency ~ 0.7). When these parameters

change, the divertor temperature and density change accordingly. Once the high recycling condition is satisfied, then the density just in front of the divertor plate and hence recycling there increases dramatically. This needs to be accompanied by increase in the plugging efficiency to avoid excessive neutral flux into the main plasma region. Otherwise high neutral flux chokes the core plasma. For the plugging calculation in Fig.8, it increases weakly with divertor density and saturates around 0.7. This estimation of the plugging efficiency take into account ionization only in the divertor channel within the divertor chamber. More meaningful plugging efficiency should includes ionization in the edge surface layers, as discussed above. The effective thickness of the edge surface multi-layers is ~ 50 mm at the high field side edge and much wider(~100 mm) near the "X-point". The neutral particles leaked from the divertor chamber are likely to be ionized in the thin curved layers near the X-point. If 60% of the leaked neutrals are ionized there, the overall plugging efficiency becomes 90 % provided that the plugging efficiency within the divertor chamber is 70 %. In the DIIID tokamak divertor experiments with plugging efficiency of 90 %, a successful operation of the high recycling mode has been achieved [10]. Since high plugging efficiency of ~90 % can be achievable in the LHD divertor configuration, we are confident that a successful high recycling operation will be realized in the LHD.

High recycling operation will enhance the edge impurity radiative power because the high density cold divertor plasma with a certain amount of impurity concentration is very effective radiator. But usually the radiative volume is not large enough to radiate away the total heat flow for the high power discharge. In the LHD configuration, there exist a fairly large volume of the open plasma region, namely edge surface layers and the stochastic region, which can be utilized as a radiative zone. With external resonant helical fields, even the volume of the stochastic region can be adjusted in such a way that nearly 100 % of the total heat flow is converted into the edge

radiative power (ergodic radiative boundary [11,12]). Whether such a scheme works or not depend on the impurity transport, particularly in the edge region. We expect that in the divertor channel, including the outer part of the edge surface layers, the friction due to the plasma flow is strong enough to sweep the impurities towards the divertor plates. In the stochastic region, it is difficult to predict transport of the impurity. But a positive electric field, expected to appear because of high electron transport in the stochastic region will hopefully provide favorable impurity transport.

High Temperature Divertor Plasma Operation

A high temperature divertor plasma operation has been proposed to improve the energy confinement of tokamaks and helical devices [13,14]. In this operational mode, the divertor plasma temperature is raised by efficient pumping in the divertor chamber. An elevated divertor temperature will lead to improvement of the core plasma. We first discuss why low recycling operation leads to enhancement in τ_E. Then the basic concept and various features of the low recycling operation are discussed.

It is difficult to discuss the heat transport since no reliable anomalous transport theory is available yet. It tends to be inevitably speculative. Our argument on why the energy confinement improves by the low recycling operation is based upon the tokamak experimental observations. We first assume that the transport mechanism in the helical system is essentially the same as in the tokamaks since the global τ_E scaling in the tokamak [15] is very similar to the LHD τ_E scaling [3]. In tokamak L-mode limiter discharges, the temperature appears to saturate at high power, a severe deterioration of the energy confinement. We consider a H-mode divertor discharge which has the same basic plasma parameters such as magnetic field, the average density as a L-mode limiter discharge except for the temperature profile. When we compare these L and H mode discharges (the main difference between them is the edge configuration), the H-mode temperature profile at the power level

just above the H-mode threshold power appears to be above that of the L-mode discharge at very high power, as illustrated in Fig. 9(a) . This is consistent with a local transport model (a very natural assumption) in which the local transport coefficients are determined by the local plasma parameters. If the L-mode profile at high power overlaps with that of the H-mode at low power, then the transport coefficient with the nearly same plasma parameters has two quite different values, contradictory to the local transport model. This argument suggest that there exists an improved confinement regime in the higher temperature parameter space. The question is how to get access to the regime. Supposed that the temperature is raised above the L-mode saturated temperature in the central region, the locally elevated temperature would drop rapidly because of the very high thermal conductivity around the boundary of the two confinement regimes, as illustrated in Fig.9(b). Thus access into the high temperature good confinement regime from the interior is almost prohibited. But when the very edge temperature is raised by the external mean such as divertor pumping (for the H-mode case, possibly by shear flow generated by the radial electric field [16]), then the discharge could enter the good confinement regime smoothly, as shown in Fig.9(c). For this case, high thermal conductivity in the L-regime does not prevent the transition to the high confinement regime. If this argument is correct, then the edge temperature needed for τ_E improvement is the order of the H-mode pedestal temperature (300 ~ 400 eV for ASDEX and DIIID, ~1 kev for JET). Recent JT60-U results [17] seem to support this argument. The energy confinement in JT60-U devices improves with decreasing particle flux to the divertor plates regardless of H or L mode.

In the high temperature divertor plasma operation mode, the edge temperature is kept high by the pumping. The divertor temperature (T_{div}) is estimated by a power balance in the divertor channel. We consider a steady-state discharge which is heated (Q_{in}(input power)) and fuelled (

Γ_{in} (particle flux)) by neutral beam injection alone. We assumed that the pumping efficiency of the divertor is ξ , i.,e., a fraction (ξ) of the particles reaching the divertor plates (Γ_{div}) are pumped and the same amount of the particles need to be fuelled by the neutral beam injection i.e, $\xi \cdot \Gamma_{div} = \Gamma_{in}$. The injected power (Q_{in}) into the main plasma region flows into the divertor channel and at the sheath of the divertor plate, a power balance ($Q_{in} = \gamma \cdot T_{div} \cdot \Gamma_{div}$) is satisfied where γ is the heat transmission coefficient. From these relations, the divertor temperature is given as $T_{div} = (Q_{in} / \Gamma_{in}) \cdot \xi / \gamma$. For a parameter set (beam energy (Q_{in} / Γ_{in}) ~ 250 kev, $\gamma \sim 10$, $\xi \sim 0.2$), T_{div} becomes as high as 5 keV, significantly higher than those observed at the pedestal of H-mode discharges.

In this operation, a peaked density profile is maintained by a combination of deep fuelling such as pellet or neutral beam injection and particle pumping. Thus the diffusion coefficient (D) and hence the particle confinement becomes important in determining the energy confinement. This is desirable for energy confinement in LHD where high neoclassical ripple induced electron heat loss(1/ν-regime) tends to suppress the temperature gradient. However the effective D is not high because the ions are well confined by E x B drift (ν-regime). The radial electric field in such a plasma regime is positive and hence neoclassical outward impurity pinch [18] may prevent the impurity contamination. When this operation is applied to tokamaks, the direction of the neoclassical impurity pinch is inward and thus the impurity accumulation could be the major problem.

The major uncertainty of this scheme is the wall plasma interaction at high plasma temperature and its associated impurity contamination.

Physical sputtering yield of D^+ ion to carbon tile has a peak value of ~ 2 % at the incident energy of ~ 200 eV. Beyond this temperature, it gradually decreases down to 0.5 % at 5 keV. Considering that the total particle flux to the divertor plate is one or two order of magnitude lower than the conventional operation, physical sputtering due to D+ ion bombardment is not a problem. The issue may be unipolar arking, which was once considered as a major impurity source in tokamak devices. It might occur at high divertor plasma temperature and definitely an experimental test for it is needed. Recent results from low recycling tokamak divertor operations (JET[19], JT60-U [17]) are very encouraging, fairly high ion temperature in the divertor channel has been observed without any severe impurity problem.

At temperature above 100 eV, secondary electrons emitted from the divertor plate become a source of the cold particles, which lower the divertor plasma temperature. This effect can be included in γ [20] and γ is ~ 7 without secondary electron emission and is ~10 when the secondary emission rate is 0.7. But when it exceeds 0.7, γ increases rapidly and then saturates at ~20 because of the space charge limit. Thus selection of the divertor plate material in terms of secondary emission is important. When divertor plasma electrons become collisionless, i.e. the electron mean free path is much longer than the field line length between the divertor plates, secondary electrons emitted from the divertor are first trapped barely by the sheath potential and makes oscillatory motion between the divertor plates. They eventually hit the divertor plate during the thermalization process. The parallel energy with which the secondary electrons hit the plates is ~ 0 and the perpendicular average energy is a fraction of the sheath potential in contrast to the previous collisional

model where both average striking energy are equal to T_e (the electron temperature). Thus the collisionless effect may reduce edge plasma cooling by secondary electrons and hence γ significantly.

In summary, the conceptional design of the LHD helical divertor has almost been completed with improved physics understanding of the divertor plasma behavior in the LHD configuration. We are now in a phase to design the hardware of the divertor components.

ACKNOWLEDEMENTS

We would like to express our particular appreciation to Drs. J. Todoroki, T. Obiki and T. Mizuuchi for valuable discussions throughout this study.

REFERENCES

[1] IIYOSHI,A., FUJIWARA, M., MOTOJIMA, O., OHYABU, N. and YAMAZAKI, Fusion Technology 17 (1990) 169.

[2] MOTOJIMA,O., AKAISHI,K., FUJII,K., FUJIWAKA, S., IMAGAWA,S., et al., Fusion Engineering and Design 20 (1993) 3.

[3] SUDO,S., TAKEIRI,Y., ZUSHI,H., SANO,F., ITOH,K., et al., Nucl. Fusion 30 (1990) 11.

[4] OHYABU,N., Nucl. Fusion 21 (1981) 519.

[5] M.ALI,MAHDAVI, DEBOO,J.C., HSIEH,C.L., OHYABU,N., STAMBAUGH,R.D., WESLEY,J.C., Phys. Rev. Lett. 47 (1981) 1602.

[6] OHYABU,N., DEBOO,J.C., GROEBNER,R.J., MAHDAVI,M.ALI, TAYLOR,T., WESLEY,J.C., Nucl. Fusion 23 (1983) 295.

[7] WAGNER,F., FUSSMANN,G., GRAVE,T., et al., Phys. Rev. Lett. 53 (1984) 1453.

[8] TODOROKI, J, Private Communication 1989.

[9] HEIFETZ,D., J. Comput. Phys. 42 (1982) 309.

[10] ALLEN,S.L.,RENSINK,M.E.HILL,D.,N.,PERKINS,D.,E., JACKSON,G.L., ALI MAHDAVI,M., J. Nucl. Mater. 162-164 (1989) 80.

[11] OHYABU,N., deGRASSIE,J.S., BROOKS,N., TAYLOR,T., IKEJI,H., et al., Nucl. Fusion 25 (1985) 1984.

[12] GROSSMAN,A., GHENDRICH,P., DEMICHELIS,C., MONIER-GARBET,P., VALLET,J.,C., et al., J. Nucl. Mater. 196-198 (1992) 59.

[13] OHYABU,N., NODA,N., JI HANTAO, AKAO,H., AKAISHI, K., et al., J. Nucl. Mater. 196-198 (1992) 276.

[14] OHYABU,N., YAMAZAKI,K., KATANUMA,I., JI,H., WATANABE, T., et al., in Plasma Physics and Controlled Nuclear Fusion Research 1992, IAEA-CN-56 / C-4-2.

[15] GOLDSTON,R., Plasma Phys. Contr. Fusion 26 (1985) 65.

[16] BIGLARI,H., DIAMOND, P.H., TERRY,P.W., Phys. Fluids B2 (1989) 1.

[17] SHIMADA, M., in Plasma Physics and Controlled Nuclear Fusion Research 1992, IAEA-CN-56 / A-1-3.

[18] SHAING,K.S., Phys. Fluids 26 (1983) 3164.

[19] WEISEN,H., BERGSAKER,H., CAMPBELL,D.J., ERENTS,S.K., deKOCK,L.C.J.M., et al., Nucl. Fusion 31 (1991) 2247.

[20] HOBBS,G.D., WESSON, J.A., Plasma Physics 9 (1967) 85.

FIGURE CAPTIONS

FIG. 1 (a) Schematic view of the LHD divertor (poloidal plane at $\phi = 18^{\circ}$) Edge magnetic structure is shown by a puncture plot of the field lines. To show a clear structure of the thin curved layer, the coil parameters are chosen to be : $\gamma_c = 1.20$, $\alpha_c = 0.0$, $\Delta = 0.0$ m, different from the LHD parameters.

(b) Crossectional view of the LHD helical divertor (perpendicular to the helical direction) at $\theta = \pi / 2$.

(c) The normalized field distribution plot on the same plane as (b).

FIG. 2 (a) Radial location of the X-point.

FIG. 3 (a) Edge surface layer (at $\phi = 18^{\circ}$) generated by tracing the field line along the B direction (forwards).

(b) An illustration of the field line movement in the edge surface layer.

FIG. 4 The connection length is plotted as a function of the starting position (3350 mm < R < 3470 mm) on the midplane (Z = 0). The sharp peaks corresponds to the edge surface layers.

FIG. 5 Puncture plots of the field lines on a helical curved surface (defined by $\theta = -[\, 5\phi + \theta_0 + 0.1 \sin(5\phi+\theta_0) \,]$ shown in Fig. 6(b). The poloidal angle difference between the surface and the helical coil center surface is 57° for three different random walk parameters.

FIG. 6 Change in the width of the thin curved layer region when the plasma axis (Δ) is changed.

FIG. 7 Radial build between the helical coil and the outermost edge surface layer on the small major radius side of the torus at $\phi = 0^{o}$.

FIG. 8 Plugging efficiency of the LHD divertor.

(a) A model configuration which simulates the LHD divertor geometry.

(b) η(plugging efficiency) as a function of n_{div}(the divertor density). Δ_p(the thickness of the divertor plasma) = 2.5 cm, Δ_{slit}(the width of the divertor entrance) =6.0 cm, d(the depth of the divertor chamber) = 15 cm.

(c) η as a function of Δ_{slit}. ($n_{div} = 1x10^{13}$ cm^{-3}, $\Delta_p = 2.5$ cm).

FIG. 9 (a) Schematic saturated temperature profiles for the L-mode at the high power and the H-mode just above the H-mode power threshold.

(b) Shrinkage of the H-mode region when the H-mode region appear in the central region,

(c) Expansion of the H-mode regime when it starts from the very edge.

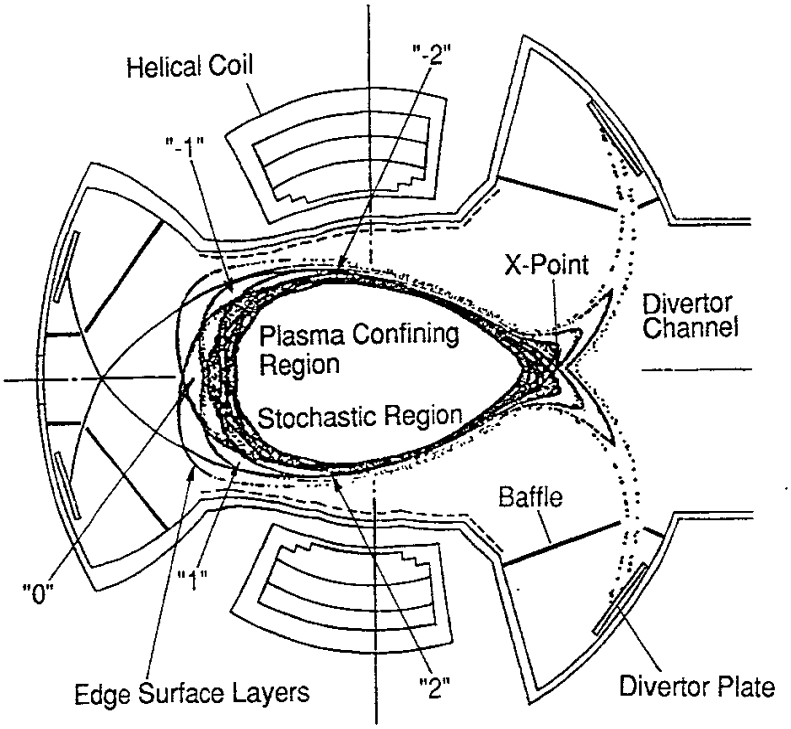
Helical Coil
"-2"
"-1"
X-Point
Divertor
Channel
Plasma Confining
Region
Stochastic Region
Baffle
"0"
"1"
Edge Surface Layers
"2"
Divertor Plate

(a)

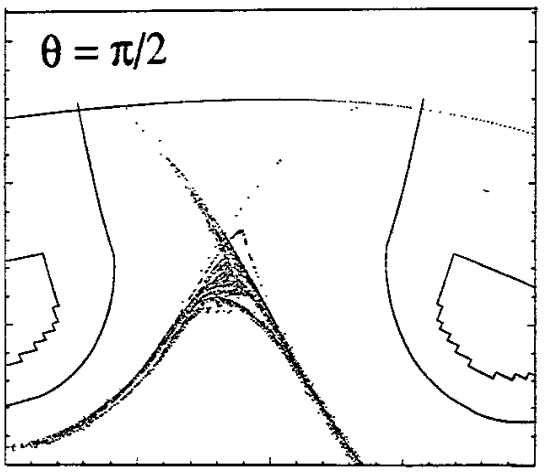
θ = π/2

(b)

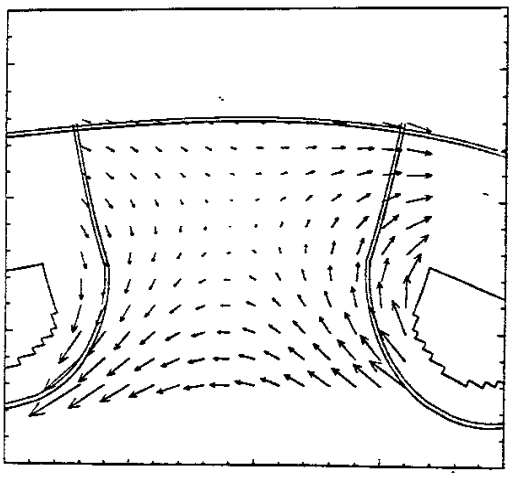

(c)

Fig.1

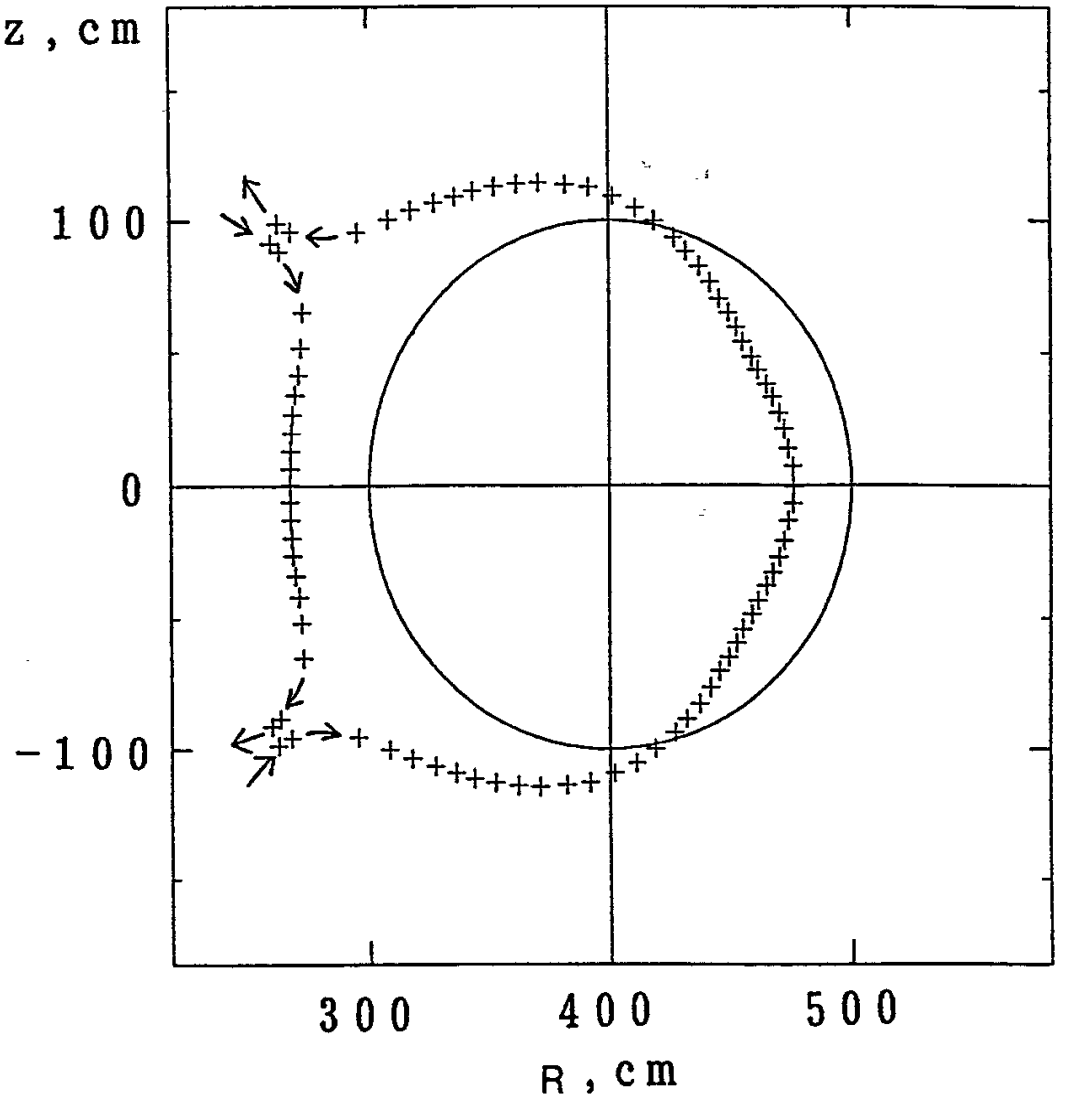

Fig.2

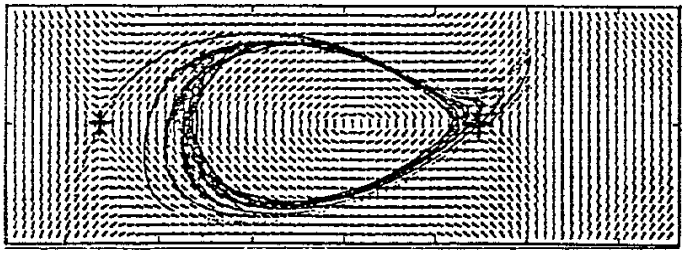

(a)

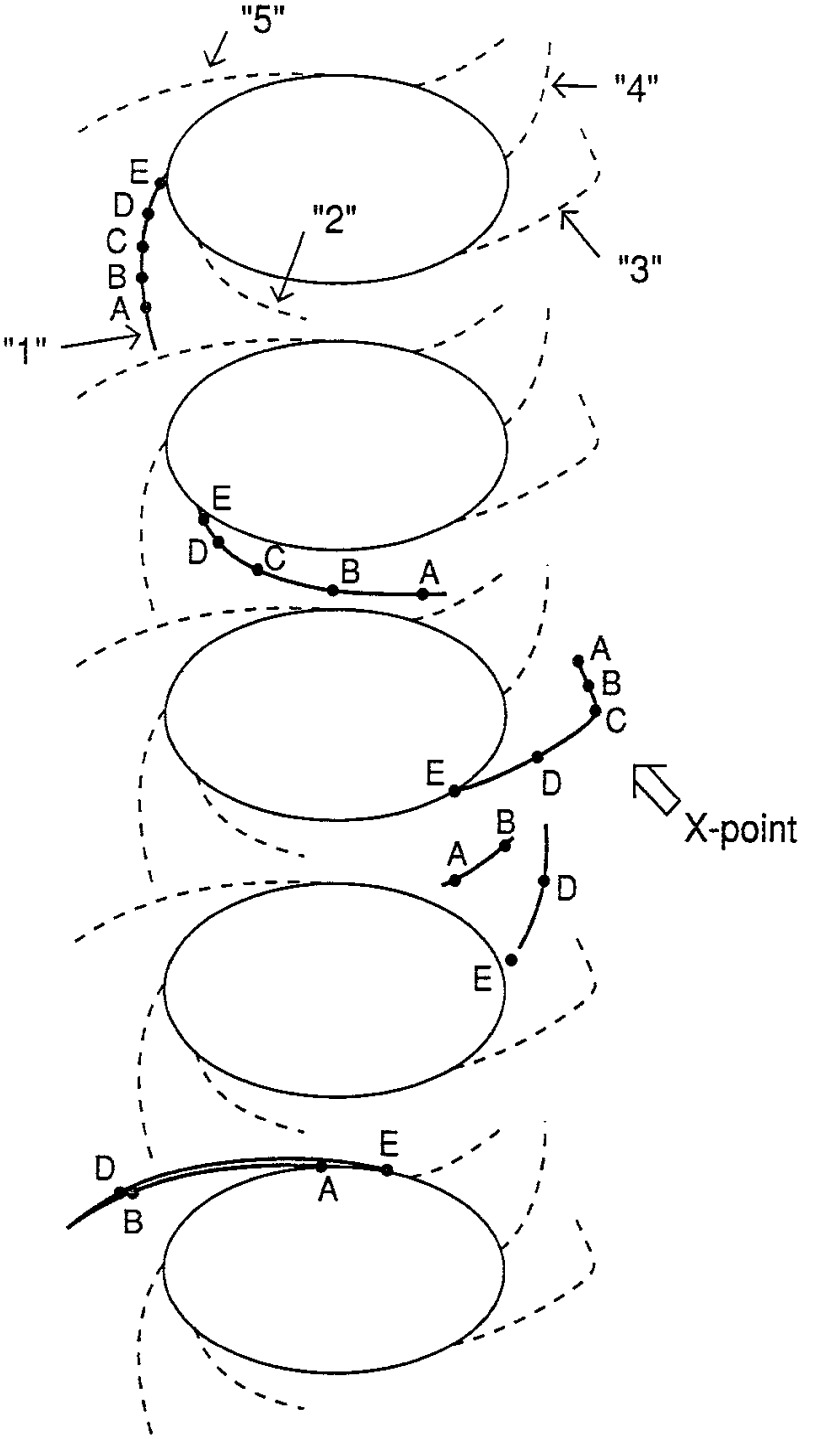

(b)

Fig.3

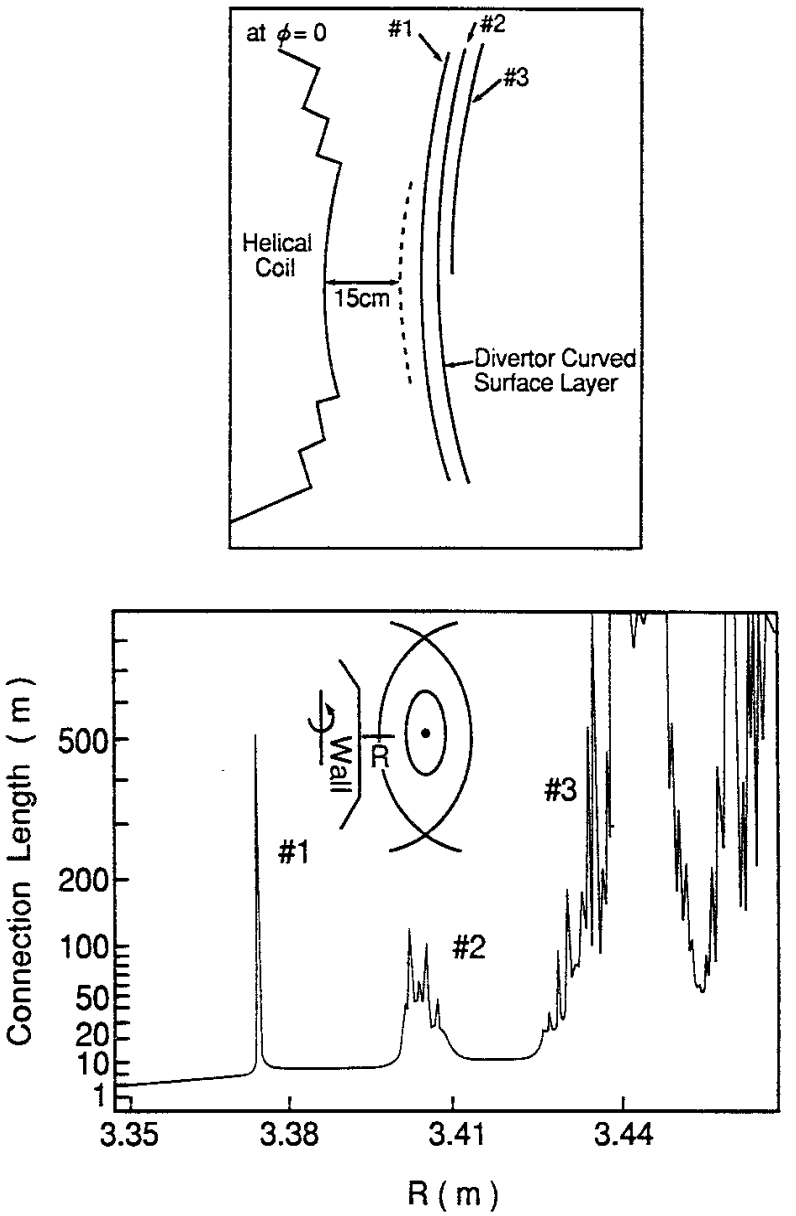
at $\phi = 0$
#1
#2
#3
Helical Coil
15cm
Divertor Curved Surface Layer
Connection Length (m)
500
200
100
50
20
10
1
Wall
R
#1
#2
#3
3.35
3.38
3.41
3.44
R (m)

Fig.4

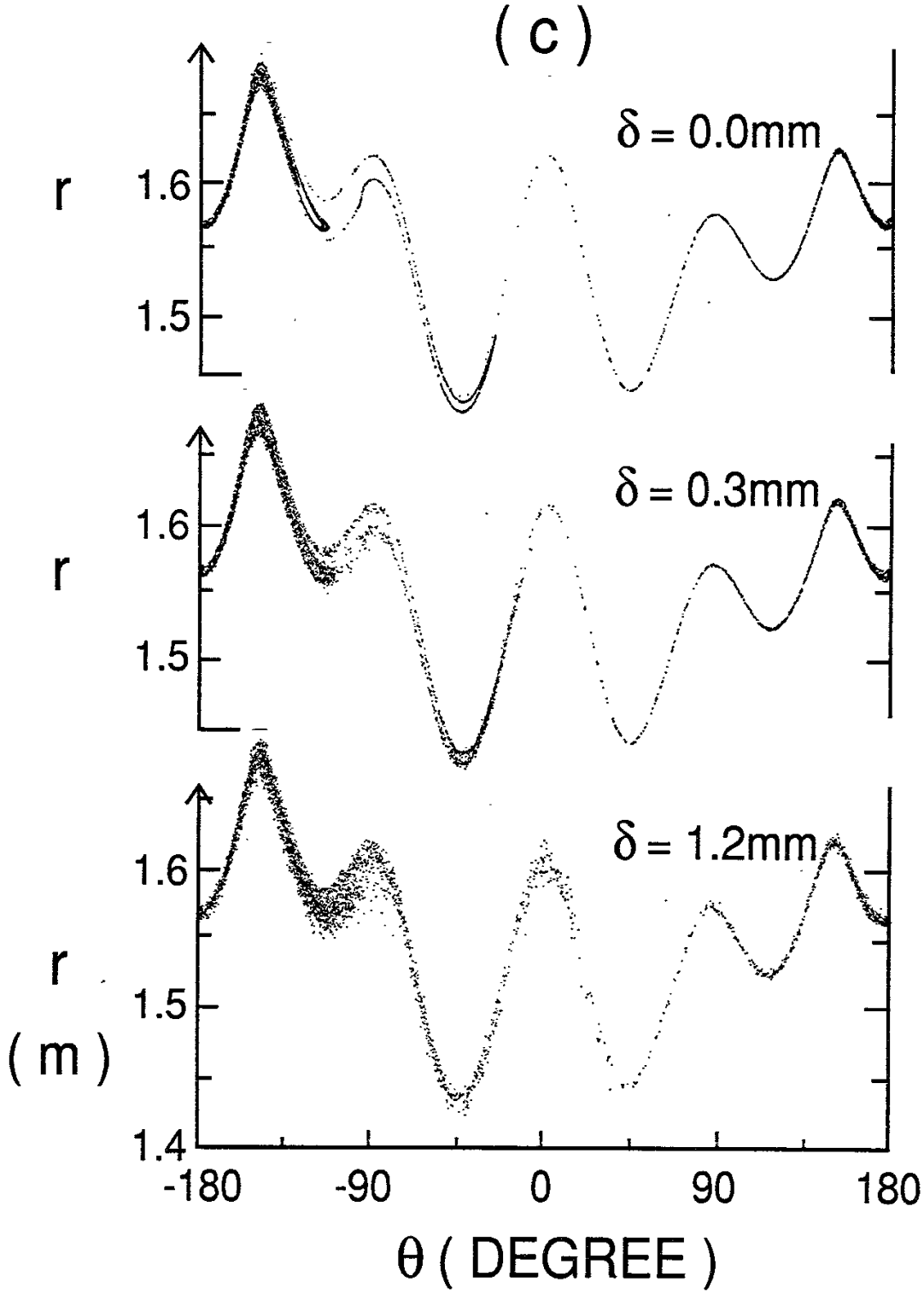

Fig.5

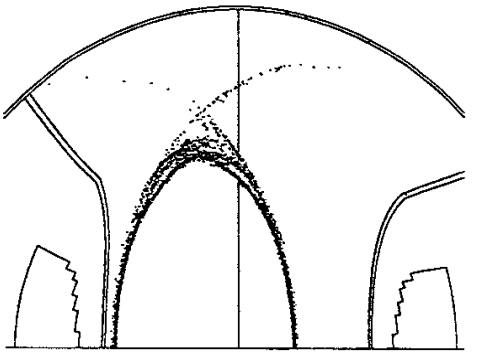

(a) $\Delta = -0.20$ m

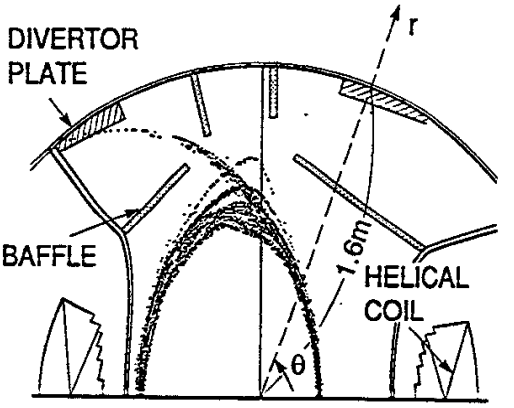

(b) $\Delta = -0.15$ m

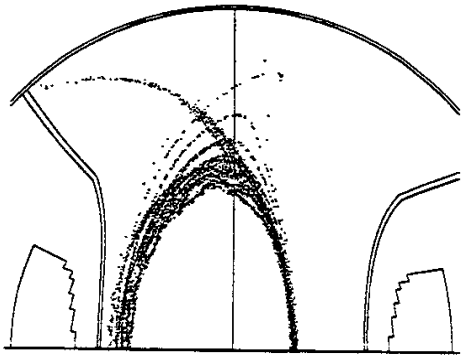

(c) $\Delta = 0.0$ m

Fig.6

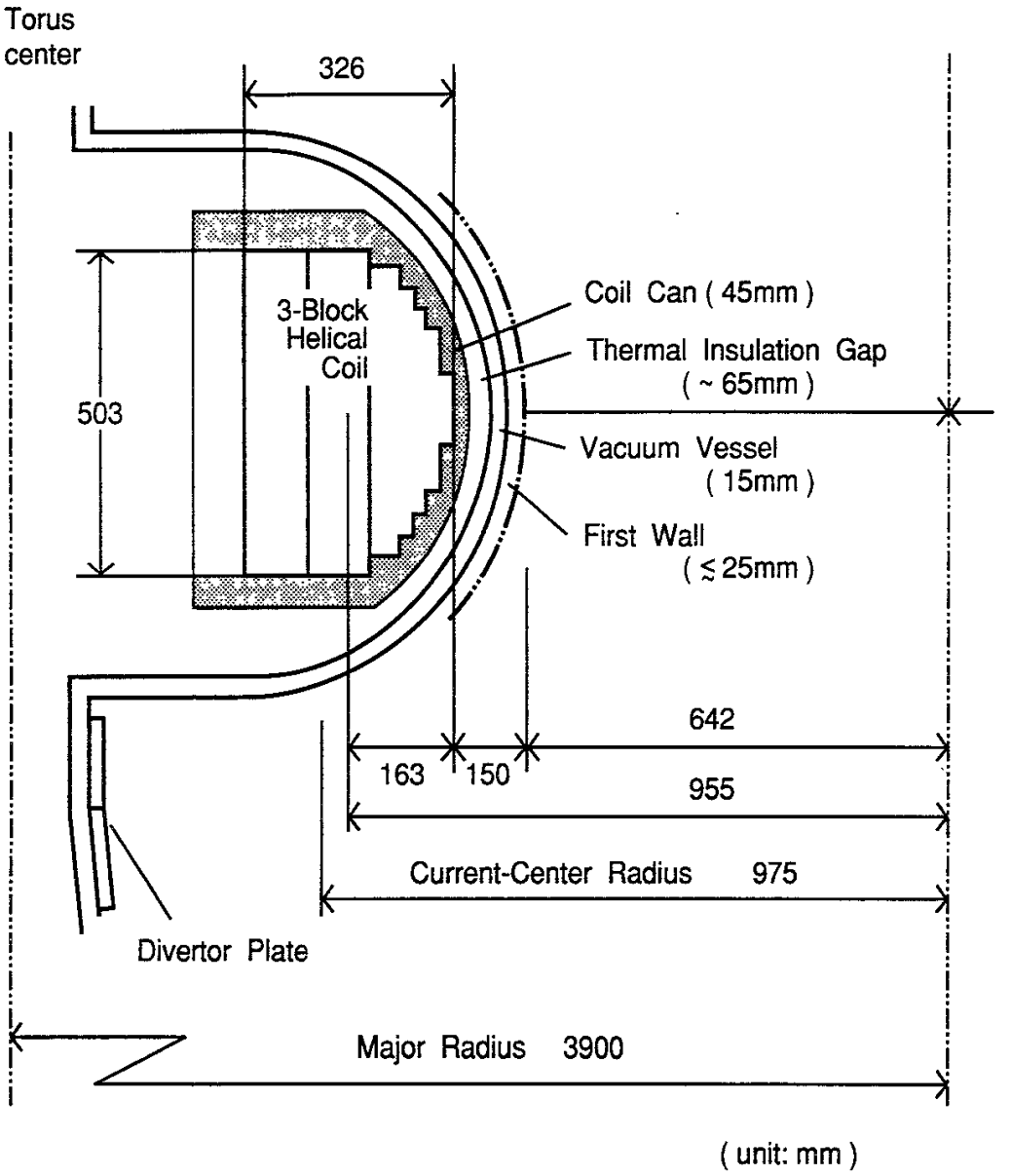
Torus
center
326
503
3-Block
Helical
Coil
Coil Can (45mm)
Thermal Insulation Gap
(~ 65mm)
Vacuum Vessel
(15mm)
First Wall
(≲ 25mm)
642
163
150
955
Current-Center Radius 975
Divertor Plate
Major Radius 3900
(unit: mm)

Fig.7

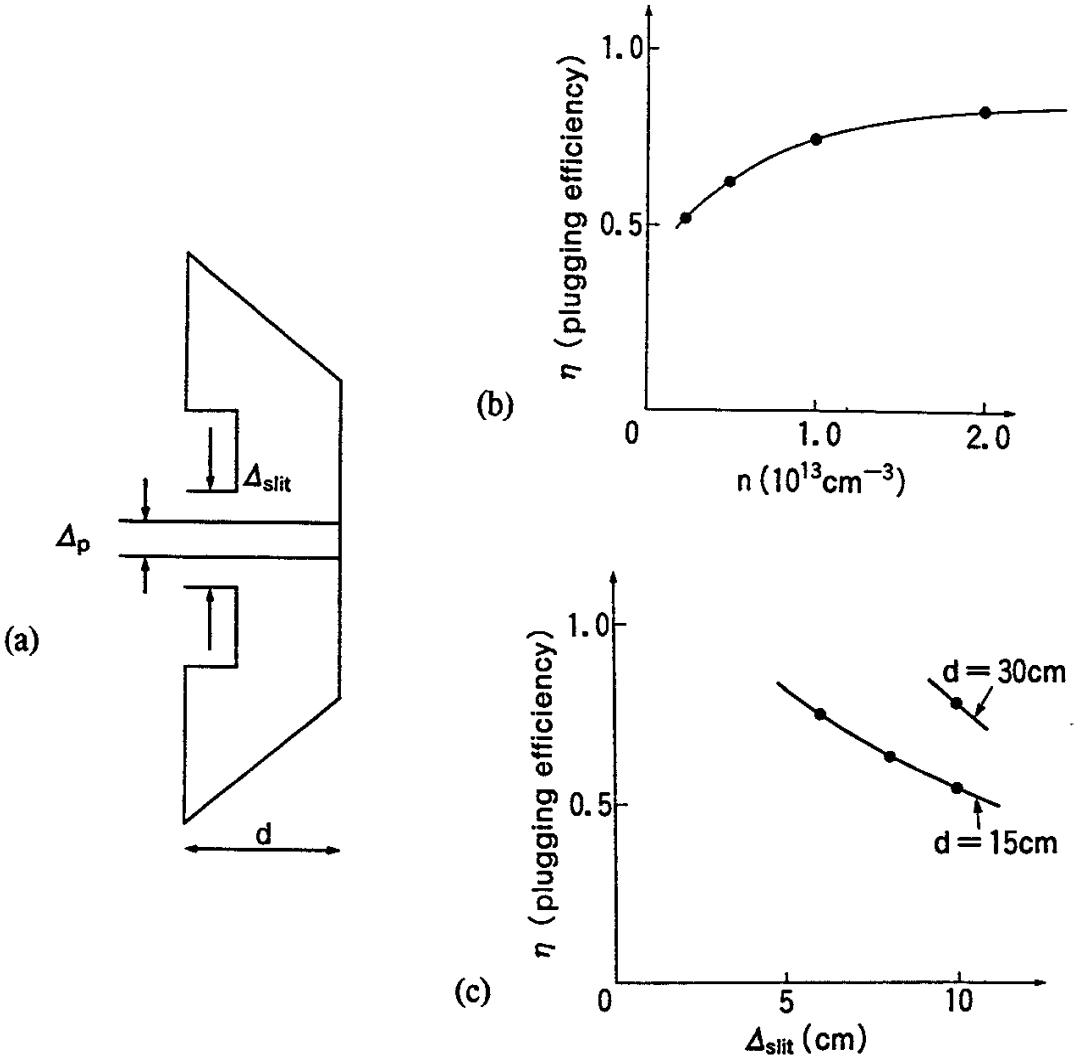
(a)
Δ_{slit}
Δ_p
d
(b)
1.0
0.5
0
1.0
2.0
η (plugging efficiency)
n (10^{13}cm^{-3})
(c)
1.0
0.5
0
5
10
η (plugging efficiency)
Δ_{slit} (cm)
d = 30cm
d = 15cm

Fig.8

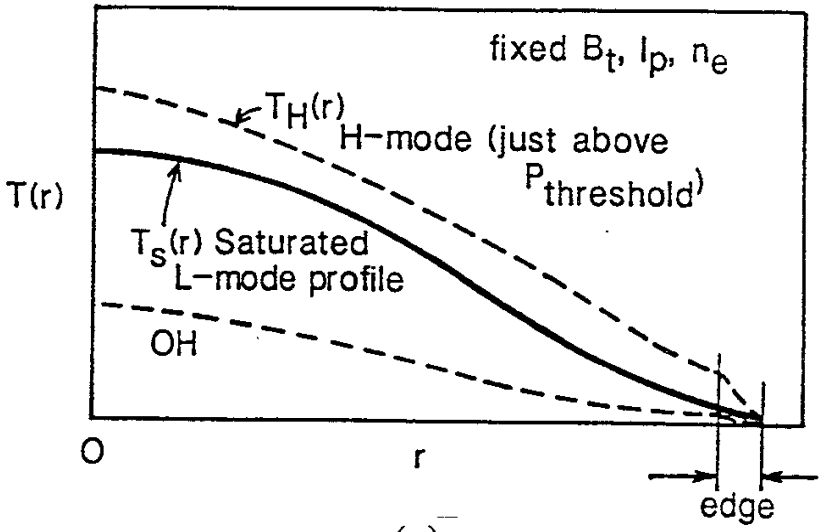
fixed B_t, I_p, n_e
$T_H(r)$
H-mode (just above $P_{threshold}$)
T(r)
$T_s(r)$ Saturated L-mode profile
OH
O
r
edge

(a)

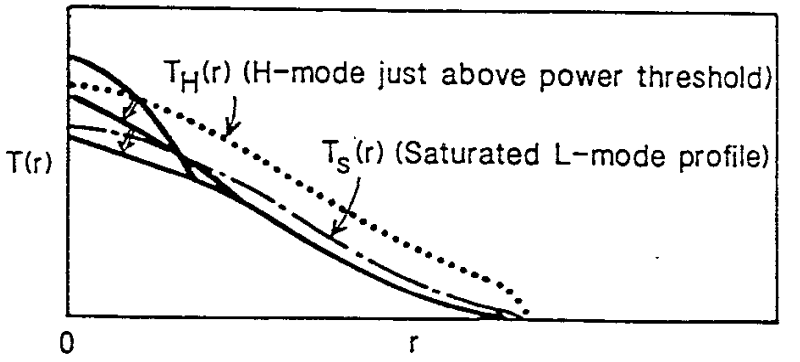
$T_H(r)$ (H-mode just above power threshold)
T(r)
$T_s(r)$ (Saturated L-mode profile)
0
r

(b)

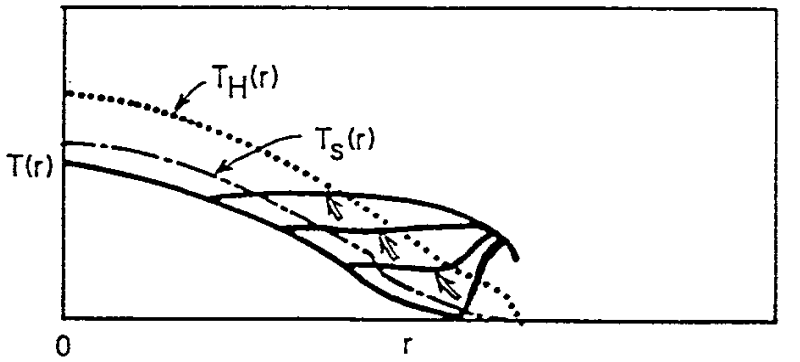
$T_H(r)$
$T_s(r)$
T(r)
0
r

(c)

Fig.9

Recent Issues of NIFS Series

NIFS-187 K. Ioth, S.-I. Itoh, A. Fukuyama, M. Yagi and M. Azumi, *Model of the L-Mode Confinement in Tokamaks* ; Sep. 1992

NIFS-188 K. Itoh, A. Fukuyama and S.-I. Itoh, *Beta-Limiting Phenomena in High-Aspect-Ratio Toroidal Helical Plasmas*; Oct. 1992

NIFS-189 K. Itoh, S. -I. Itoh and A. Fukuyama, *Cross Field Ion Motion at Sawtooth Crash* ; Oct. 1992

NIFS-190 N. Noda, Y. Kubota, A. Sagara, N. Ohyabu, K. Akaishi, H. Ji, O. Motojima, M. Hashiba, I. Fujita, T. Hino, T. Yamashina, T. Matsuda, T. Sogabe, T. Matsumoto, K. Kuroda, S. Yamazaki, H. Ise, J. Adachi and T. Suzuki, *Design Study on Divertor Plates of Large Helical Device (LHD)* ; Oct. 1992

NIFS-191 Y. Kondoh, Y. Hosaka and K. Ishii, *Kernel Optimum Nearly-Analytical Discretization (KOND) Algorithm Applied to Parabolic and Hyperbolic Equations* : Oct. 1992

NIFS-192 K. Itoh, M. Yagi, S.-I. Itoh, A. Fukuyama and M. Azumi, *L-Mode Confinement Model Based on Transport-MHD Theory in Tokamaks* ; Oct. 1992

NIFS-193 T. Watari, *Review of Japanese Results on Heating and Current Drive* ; Oct. 1992

NIFS-194 Y. Kondoh, *Eigenfunction for Dissipative Dynamics Operator and Attractor of Dissipative Structure* ; Oct. 1992

NIFS-195 T. Watanabe, H. Oya, K. Watanabe and T. Sato, *Comprehensive Simulation Study on Local and Global Development of Auroral Arcs and Field-Aligned Potentials* ; Oct. 1992

NIFS-196 T. Mori, K. Akaishi, Y. Kubota, O. Motojima, M. Mushiaki, Y. Funato and Y. Hanaoka, *Pumping Experiment of Water on B and LaB_6 Films with Electron Beam Evaporator* ; Oct., 1992

NIFS-197 T. Kato and K. Masai, *X-ray Spectra from Hinotori Satellite and Suprathermal Electrons* ; Oct. 1992

NIFS-198 K. Toi, S. Okamura, H. Iguchi, H. Yamada, S. Morita, S. Sakakibara, K. Ida, K. Nishimura, K. Matsuoka, R. Akiyama, H. Arimoto, M. Fujiwara, M. Hosokawa, H. Idei, O. Kaneko, S. Kubo, A. Sagara, C. Takahashi, Y. Takeiri, Y. Takita, K. Tsumori, I. Yamada and

H. Zushi, *Formation of H-mode Like Transport Barrier in the CHS Heliotron / Torsatron* ; Oct. 1992

NIFS-199 M. Tanaka, *A Kinetic Simulation of Low-Frequency Electromagnetic Phenomena in Inhomogeneous Plasmas of Three-Dimensions* ; Nov. 1992

NIFS-200 K. Itoh, S.-I. Itoh, H. Sanuki and A. Fukuyama, *Roles of Electric Field on Toroidal Magnetic Confinement*, Nov. 1992

NIFS-201 G. Gnudi and T. Hatori, *Hamiltonian for the Toroidal Helical Magnetic Field Lines in the Vacuum*; Nov. 1992

NIFS-202 K. Itoh, S.-I. Itoh and A. Fukuyama, *Physics of Transport Phenomena in Magnetic Confinement Plasmas*; Dec. 1992

NIFS-203 Y. Hamada, Y. Kawasumi, H. Iguchi, A. Fujisawa, Y. Abe and M. Takahashi, *Mesh Effect in a Parallel Plate Analyzer*; Dec. 1992

NIFS-204 T. Okada and H. Tazawa, *Two-Stream Instability for a Light Ion Beam -Plasma System with External Magnetic Field;* Dec. 1992

NIFS-205 M. Osakabe, S. Itoh, Y. Gotoh, M. Sasao and J. Fujita, *A Compact Neutron Counter Telescope with Thick Radiator (Cotetra) for Fusion Experiment*; Jan. 1993

NIFS-206 T. Yabe and F. Xiao, *Tracking Sharp Interface of Two Fluids by the CIP (Cubic-Interpolated Propagation) Scheme*, Jan. 1993

NIFS-207 A. Kageyama, K. Watanabe and T. Sato, *Simulation Study of MHD Dynamo : Convection in a Rotating Spherical Shell*; Feb. 1993

NIFS-208 M. Okamoto and S. Murakami, *Plasma Heating in Toroidal Systems*; Feb. 1993

NIFS-209 K. Masai, *Density Dependence of Line Intensities and Application to Plasma Diagnostics*; Feb. 1993

NIFS-210 K. Ohkubo, M. Hosokawa, S. Kubo, M. Sato, Y. Takita and T. Kuroda, *R&D of Transmission Lines for ECH System* ; Feb. 1993

NIFS-211 A. A. Shishkin, K. Y. Watanabe, K. Yamazaki, O. Motojima, D. L. Grekov, M. S. Smirnova and A. V. Zolotukhin, *Some Features of Particle Orbit Behavior in LHD Configurations*; Mar. 1993

NIFS-212 Y. Kondoh, Y. Hosaka and J.-L. Liang, *Demonstration for Novel Self-organization Theory by Three-Dimensional Magnetohydrodynamic Simulation*; Mar. 1993

NIFS-213 K. Itoh, H. Sanuki and S.-I. Itoh, *Thermal and Electric Oscillation Driven by Orbit Loss in Helical Systems*; Mar. 1993

NIFS-214 T. Yamagishi, *Effect of Continuous Eigenvalue Spectrum on Plasma Transport in Toroidal Systems*; Mar. 1993

NIFS-215 K. Ida, K. Itoh, S.-I.Itoh, Y. Miura, JFT-2M Group and A. Fukuyama, *Thickness of the Layer of Strong Radial Electric Field in JFT-2M H-mode Plasmas*; Apr. 1993

NIFS-216 M. Yagi, K. Itoh, S.-I. Itoh, A. Fukuyama and M. Azumi, *Analysis of Current Diffusive Ballooning Mode*; Apr. 1993

NIFS-217 J. Guasp, K. Yamazaki and O. Motojima, *Particle Orbit Analysis for LHD Helical Axis Configurations* ; Apr. 1993

NIFS-218 T. Yabe, T. Ito and M. Okazaki, *Holography Machine HORN-1 for Computer-aided Retrieve of Virtual Three-dimensional Image* ; Apr. 1993

NIFS-219 K. Itoh, S.-I. Itoh, A. Fukuyama, M. Yagi and M. Azumi, *Self-sustained Turbulence and L-Mode Confinement in Toroidal Plasmas* ; Apr. 1993

NIFS-220 T. Watari, R. Kumazawa, T. Mutoh, T. Seki, K. Nishimura and F. Shimpo, *Applications of Non-resonant RF Forces to Improvement of Tokamak Reactor Performances Part I: Application of Ponderomotive Force* ; May 1993

NIFS-221 S.-I. Itoh, K. Itoh, and A. Fukuyama, *ELMy-H mode as Limit Cycle and Transient Responses of H-modes in Tokamaks* ; May 1993

NIFS-222 H. Hojo, M. Inutake, M. Ichimura, R. Katsumata and T. Watanabe, *Interchange Stability Criteria for Anisotropic Central-Cell Plasmas in the Tandem Mirror GAMMA 10 ;* May 1993

NIFS-223 K. Itoh, S.-I. Itoh, M. Yagi, A. Fukuyama and M. Azumi, *Theory of Pseudo-Classical Confinement and Transmutation to L-Mode;* May 1993

NIFS-224 M. Tanaka, *HIDENEK: An Implicit Particle Simulation of Kinetic-MHD Phenomena in Three-Dimensional Plasmas;* May 1993

NIFS-225 H. Hojo and T. Hatori, *Bounce Resonance Heating and Transport in a Magnetic Mirror;* May 1993

NIFS-226 S.-I. Iton, K. Itoh, A. Fukuyama, M. Yagi, *Theory of Anomalous*

Transport in H-Mode Plasmas; May 1993

NIFS-227 T. Yamagishi, *Anomalous Cross Field Flux in CHS ;* May 1993

NIFS-228 Y. Ohkouchi, S. Sasaki, S. Takamura, T. Kato, *Effective Emission and Ionization Rate Coefficients of Atomic Carbons in Plasmas;* June 1993

NIFS-229 K. Itoh, M. Yagi, A. Fukuyama, S.-I. Itoh and M. Azumi, *Comment on 'A Mean Field Ohm's Law for Collisionless Plasmas;* June 1993

NIFS-230 H. Idei, K. Ida, H. Sanuki, H. Yamada, H. Iguchi, S. Kubo, R. Akiyama, H. Arimoto, M. Fujiwara, M. Hosokawa, K. Matsuoka, S. Morita, K. Nishimura, K. Ohkubo, S. Okamura, S. Sakakibara, C. Takahashi, Y. Takita, K. Tsumori and I. Yamada, *Transition of Radial Electric Field by Electron Cyclotron Heating in Stellarator Plasmas;* June 1993

NIFS-231 H.J. Gardner and K. Ichiguchi, *Free-Boundary Equilibrium Studies for the Large Helical Device,* June 1993

NIFS-232 K. Itoh, S.-I. Itoh, A. Fukuyama, H. Sanuki and M. Yagi, *Confinement Improvement in H-Mode-Like Plasmas in Helical Systems,* June 1993

NIFS-233 R. Horiuchi and T. Sato, *Collisionless Driven Magnetic Reconnection,* June 1993

NIFS-234 K. Itoh, S.-I. Itoh, A. Fukuyama, M. Yagi and M. *Azumi, Prandtl Number of Toroidal Plasmas;* June 1993

NIFS-235 S. Kawata, S. Kato and S. Kiyokawa , *Screening Constants for Plasma;* June 1993

NIFS-236 A. Fujisawa and Y. Hamada, *Theoretical Study of Cylindrical Energy Analyzers for MeV Range Heavy Ion Beam Probes;* July 1993

NIFS-237 N. Ohyabu, A. Sagara, T. Ono, T. Kawamura and O. Motojima, *Carbon Sheet Pumping;* July 1993

NIFS-238 K. Watanabe, T. Sato and Y. Nakayama, *Q-profile Flattening due to Nonlinear Development of Resistive Kink Mode and Ensuing Fast Crash in Sawtooth Oscillations;* July 1993